Journal Homepage: http://ijcpe.uobaghdad.edu.iq
Iraqi Journal of Chemical and Petroleum Engineering
Vol. 27 No. 1 (March 2026) 67 – 83
EISSN: 2618-0707, PISSN: 1997-4884

Silica sand-supported nZVI-Cu nanoparticles synthesized in a green method for antibiotics removal from aqueous solutions

Farah Samir Mohammed [a, *], Alaa Kareem Mohammed [a], Ziad Tark Abd Ali [b]

a Biochemical Engineering Department, Al-Khwarizmi College of Engineering, University of Baghdad, Baghdad, 47024, Iraq
b Environment Engineering Department, College of Engineering, University of Baghdad, Baghdad, 47024, Iraq

Abstract

It is challenging to remove antibiotics from water bodies, as they are among the most widespread contaminants in the environment, particularly with conventional wastewater treatment methods, due to their persistence and low biodegradability. The current study examined the use of nanoscale zero-valent iron to remove antibiotics. Conocarpus leaf extract, which is primarily composed of polyphenols like flavonoids and tannins, was employed as a green source to prepare Fe/Cu nanoparticles, which can act as an eco-friendly reducing agent. The nanoparticles were immobilized onto silica sand (SS), forming SS-Fe/Cu nanocomposite to remove tetracycline (TC) and ciprofloxacin (CIP) from aqueous solutions. The structural characteristics of the produced nanocomposite were examined using a number of analytical techniques, including XRD, FTIR, FE-SEM, EDS, TEM, BET, TGA, and DSC. The structural and morphological analyses confirmed the successful synthesis of the SS–Fe/Cu nanocomposite, with well-dispersed nanoparticles (FE-SEM/TEM), characteristic functional groups (FTIR), crystalline structure (XRD), surface area enhancement (BET), elemental composition (EDS), and good thermal stability (TGA/DSC). Studies were conducted through batch experiments, and the influence of various variables (contact time, pH, agitation speed, nanocomposite dosage, and initial pollutant concentration (C_o)) was investigated. The maximum removal efficiencies of 93% and 85% were achieved for TC and CIP, respectively, under ideal conditions: time = 90 min, pH of 11 for TC and 7 for CIP, agitation speed = 200 rpm, C_o = 10 mg/L, and nanocomposite dosage of 1 g/50 mL. Isotherm, kinetic, and thermodynamic studies showed that adsorption of both TC and CIP followed the Freundlich model and pseudo-second-order kinetics, indicating chemisorption as the main mechanism. Thermodynamic results revealed that TC adsorption was endothermic and non-spontaneous (positive $\Delta S°$), while CIP adsorption was exothermic and spontaneous (negative $\Delta S°$), confirming the efficiency of the SS–Fe/Cu nanocomposite. The results revealed that the green-fabricated SS-Fe/Cu nanocomposite could be used as an efficient agent for extracting TC and CIP from aqueous solutions.

Keywords: Conocarpus leaf extract; nZVI; SS-Fe/Cu nanocomposite; Tetracycline; Ciprofloxacin; Adsorption.

Received on 25/11/2025, Received in Revised Form on 19/01/2026, Accepted on 19/01/2026, Published on 30/03/2026

https://doi.org/10.31699/IJCPE.2026.1.6

1- Introduction

The water resource deterioration caused by emerging pollutants is intensified with the population increase. Today, many different industries create large amounts of wastewater containing hazardous organic and inorganic contaminants, among them carcinogenic [1, 2]. Therefore, there is a need for an effective remediation strategy to protect water resources and keep the environment clean and suitable for human consumption [3]. Comparable to the most significant contaminants in the water system, pharmaceuticals are discharged in significant amounts due to a variety of human activities. These include effluent from sewage and water treatment facilities as well as raw sewage from residences, businesses, and hospitals [4, 5].

One of the most applied antibiotics is tetracycline (TC), which has been applied in many sectors such as agriculture, human medicine, and veterinary medicine [6, 7]. TC has a strong therapeutic effect, broad-spectrum antibacterial activity [8], and a moderate price, and is the second most commonly used kind of antibiotic worldwide [9, 10]. Due to the high fate (environmental half-life) of TC and high solubility, in the event of excess use of these, surface and groundwater quality will be severely damaged.

Ciprofloxacin (CIP) is another frequently used antibiotic. Gram-positive and gram-negative bacteria can both be combatted by this broad-spectrum antibiotic [11]. Ciprofloxacin belongs to the fluoroquinolone pharmaceutical group. Due to its antimicrobial and chemical stability, it has been widely used as an antibiotic [12, 13]. Thus, when CIP is present in the water bodies at levels greater than routine, it results in the emergence of resistant microbes, which leads to the breakage of the antibiotic chain [14].

One of the methods applied for wastewater treatment is the adsorption process. This method is considered the most commonly used method to eliminate different pollutants, such as pharmaceuticals, because it is a scalable process, easy to use, economical, low-energy

*Corresponding Author: Email: Farah.Samir1705a@kecbu.uobaghdad.edu.iq

demand, low impact on the environment, and repeatable [15, 16].

Antibiotics' persistence and low biodegradability make it difficult for traditional wastewater treatment technologies to remove them efficiently. The large surface area and potent interaction of nanoparticles with antibiotic compounds make them a potential solution that improves removal efficiency even at low concentrations [17, 18]. For the on-site remediation of both organic and inorganic contaminants, nano-scale zero valent iron (nZVI) has gained increased interest in recent years. As reported so far, nZVI is one of the best and most promising materials used to remove antibiotics in water. Due to their strength, reactivity, and abundance of reactive sites, nZVI particles can remove a wide range of antibiotics from wastewater [19]. However, despite such potential applications in bioremediation, it is important to consider the constraints of nZVI particles. Some of the difficulties involve fast aggregation, limited stability, and the absence of reagent isolation [20]. The following challenges are the primary barriers to applying nZVI in environmental remediation. To overcome these challenges, many approaches have been proposed to improve the reactivity of nZVI particles [21, 22]. Several methods, like suitable doping with other metals (Cu, Ag, Zn, and Ni), depositing stabilizing chemicals on their surface, or immobilization of the clusters over inert supports, can solve these problems [23, 24]. Dopant metals on nZVI particles were reported with several functions, such as stabilization, catalytic activity, and activation energy reduction, when dopant metals are in the coated nZVI nanoparticles [25]. The dopant metals of the bimetallic nanoparticles enhance the performance of the iron nanoparticles by promoting the activation of atomic H on the nZVI-dedicated surface [26].

Dangerous chemicals, such as borohydride ($NaBH_4$), that might be hazardous to both human beings and the environment, are frequently employed as reduction agents to create iron nanoparticles [27]. Besides, the chemical synthesis of nZVI is costly for field application. One of the most significant low-cost and environmentally friendly alternative techniques for creating nanoparticles is green synthesis, which uses plant leaf extract that is abundant in capping and reducing agents (flavonoids, polyphenols, and other reducing compounds). These agents may be used as reducing agents to convert iron salts to zero-valent and to prevent agglomeration. Additionally, it tends to stabilize nanoparticles and alter their surface characteristics [28, 29]. The Conocarpus tree has been used medicinally in many nations. It is effective against a variety of diseases such as cancers, respiratory disorders, common infections, colitis, constipation, tooth decay, and malaria [30]. Its primary components are polyphenols such as flavonoids and tannins. Conocarpus is an excellent reductive agent, and the entire process is non-toxic and eco-friendly due to its phenolic richness [31, 32]. Yet some residents have been trying to have trees removed that have led to and are causing extensive drainage problems and have broken water pipes because the trees' roots are so invasive and have travelled such long distances below the ground [30].

In this work, copper (Cu(II)) was employed as a dopant metal to synthesize bimetallic Fe/Cu nanoparticles, while silica sand was used as a low-cost support material to immobilize the nanoparticles. This strategy aims to reduce nanoparticle agglomeration, prevent surface area loss, and enhance stability, regeneration, and reusability. Furthermore, Conocarpus leaf extract was utilized as a green reducing and stabilizing agent for nanoparticle synthesis. To the best of our knowledge, the application of Conocarpus leaf extract for the green synthesis of bimetallic Fe/Cu nanoparticles has not been previously reported. The resulting silica-supported bimetallic nanocomposite (SS–Fe/Cu) was subsequently applied for the removal of tetracycline and ciprofloxacin from aqueous solutions. This green synthesis strategy, combining plant-based reduction with Cu(II) doping of nZVI and low-cost silica support, demonstrates the potential of sustainable nanotechnology for wastewater treatment applications.

2- Materials and methods

2.1. Materials

Silica sand (SS) with a 98% silica ratio was acquired from Al-Nawafeth Company's local market. The particle size ranges from 0.3 to 0.5 mm, the initial porosity is 0.45, and the specific gravity is 1.363. Ferric chloride ($FeCl_3$), copper (II) sulfate pentahydrate ($CuSO_4 \cdot 5H_2O$), hydrochloric acid (HCl), sodium hydroxide (NaOH), and absolute ethanol (99.9%) were purchased from India from CDH Fine Chemicals Company. Tetracycline ($C_{22}H_{24}N_2O_8$) and ciprofloxacin ($C_{17}H_{18}FN_3O_3$) were model analyses imported from Samarra Pharmaceuticals Factory, Iraq. Table 1 summarizes the characteristics of TC and CIP. The chemicals and reagents utilized are all of analytical grade.

Table 1. Chemical properties of TC and CIP

Property	TC	CIP
Chemical formula	$C_{22}H_{24}N_2O_8$	$C_{17}H_{18}FN_3O_3$
Molecular weight (g/mol)	444.435	331.34
Melting point (℃)	170-175	322
Chemical structure	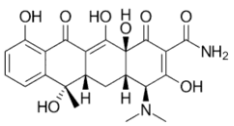	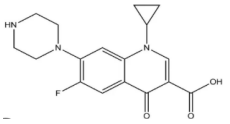
Company	Samarra Pharmaceutical Factory, Iraq	Samarra Pharmaceutical Factory, Iraq
Wavelength (nm)	357	275

2.2. Green Synthesis of SS-Fe/Cu nanocomposite

2.2.1. Conocarpus leaf extract preparation

The locally obtained Conocarpus leaves were collected and carefully washed multiple times with distilled water to get rid of dust and other impurities. Then, the leaves were dried in an oven at 70 °C for 24 h. After drying, a fine powder was prepared from the leaves with the help of a grinding machine to enhance the extraction process of the polyphenols. The dried leaves (30 g) were extracted for 4 h with distilled water (100 mL) in an ultrasonic water bath. Studies have shown that the levels of polyphenols in aqueous extracts are much greater than those obtained by alcohol [33]. The mixture was then filtered through the filter paper, and the filtrate was collected and stored at 20 °C for later use.

2.2.2. Synthesis of SS-Fe/Cu nanocomposite

Silica sand was purified by repeated washing with tap water, followed by soaking in 1 M HCl for 24 h, and subsequent rinsing with distilled water to remove impurities [34]. Bimetallic nanocomposites (SS-Fe/Cu) were synthesized according to the method in [35]. Briefly, 25 g of silica sand was mixed with 150 mL of 0.4 M $FeCl_3$ solution and agitated for 30 min at room temperature. Next, 150 mL of 0.4 M $CuSO_4.5H_2O$ solution was added in a Fe/Cu molar ratio of 1, and the mixture was shaken for 2 h to form the bimetallic nanocomposite. Finally, the nanocomposite was filtered and then dried at 70 °C overnight in an oven. A 30% Conocarpus leaf extract was then added gradually to the dried $FeCl_3$/$CuSO_4$-coated sand, resulting in the reduction of iron ions to zero-valent iron and a noticeable color shift from bright yellow to black. A 1 M NaOH solution was introduced to adjust the pH of the solution to 9. The mixture was agitated for a further half hour on an orbital shaker to guarantee complete homogeneity. After filtering and washing three times with 100% ethanol to get rid of any remaining chemicals, the SS-Fe/Cu nanocomposite was dried at 70 °C in a vacuum oven. The resulting nanocomposite was stored in a sealed container for subsequent batch experiments. Fig. 1 depicts the environmentally friendly fabrication method for the SS-Fe/Cu nanocomposite.

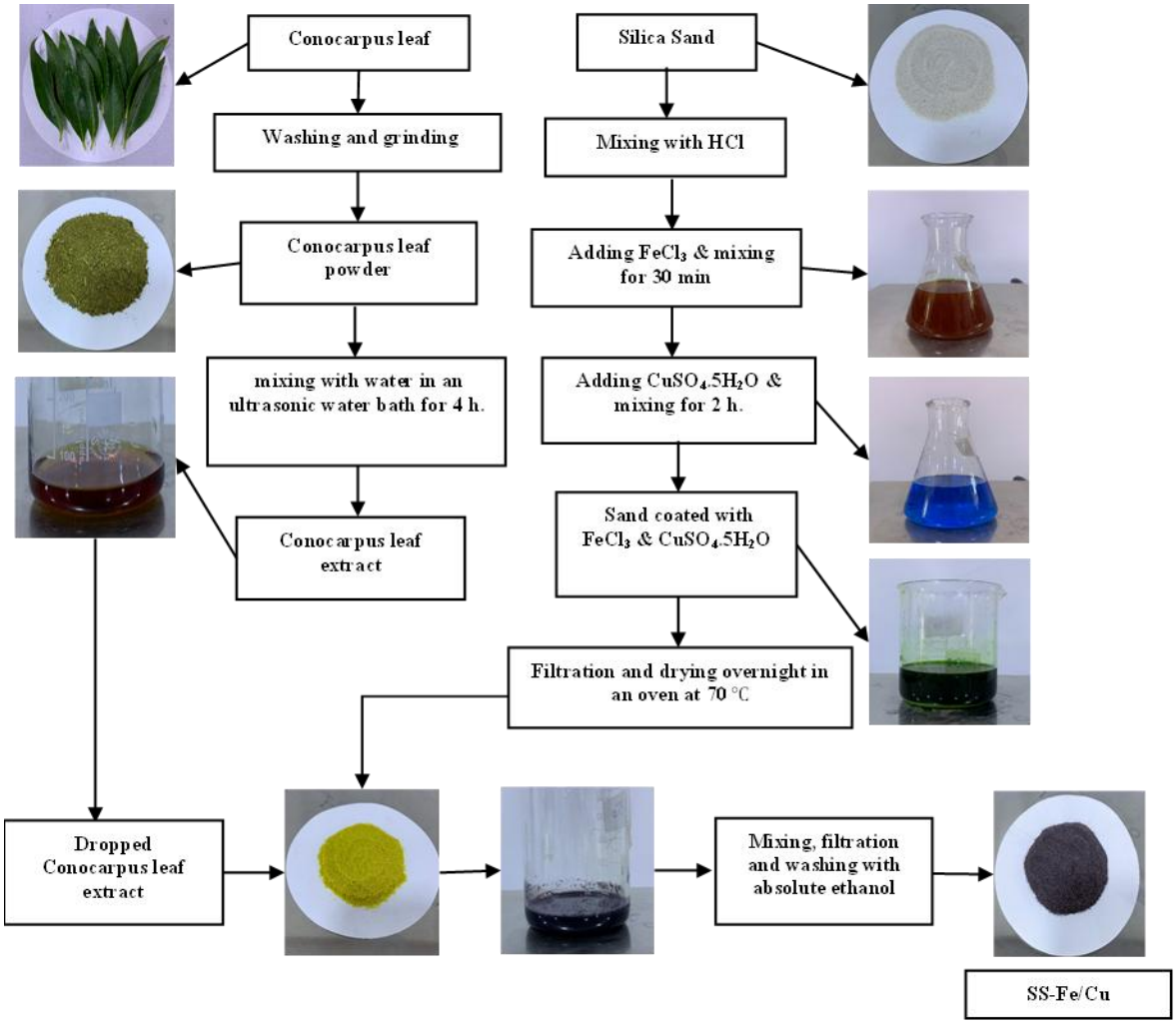

Fig. 1. Schematic diagram of SS-Fe/Cu nanocomposite green synthesis

2.3. Characterizations of SS-Fe/Cu nanocomposite

The SS-Fe/Cu nanocomposite was used in the tests after undergoing a thorough characterization. The following describes the methods used in characterization:

- X-Ray Diffraction (XRD) was used to examine the produced SS-Fe/Cu nanocomposite's crystallinity and phase composition. Using copper radiation, the scan was performed over a 2θ temperature range from 10 to 80 °C.
- To conduct spectroscopy observation, the syenthesized material's surface functional groups were examined using Fourier Transform Infrared Spectroscopy (FTIR). 400–4000 cm^{-1} was the processing range for the spectra.
- Surface morphology, structural parameters, as well as particle size distribution were determined by Field Emission Scanning Electron Microscope (FE-SEM).
- EDS analysis was used as an analytical method to elucidate surface morphologies, size distribution, and elemental composition of the synthesized nanocomposite, together with FE-SEM.
- Surface areas are important in terms of where pollutants may be associated with active sites. This was estimated by Brunauer-Emmett-Teller (BET) techniques (based on nitrogen adsorption-desorption at 77 K and 88 kPa), which showed the sample's specific surface area and pore size.
- Transmission Electron Microscopy (TEM) (Morgagni-270-D) was used to analyze the morphology of the produced nanocomposite at an acceleration voltage of 80.0 kV.
- Thermogravimetric Analysis (TGA) was used to measure the change in a sample's weight as a function of temperature, providing information about its thermal stability, decomposition behavior, and volatile content.
- Differential Scanning Calorimetry (DSC) was used to determine the heat flow associated with phase transitions or chemical reactions, allowing the evaluation of melting points, crystallization, and other thermal properties of materials.

2.4. Batch experiments

To remove TC and CIP from aqueous solutions effectively, batch adsorption experiments were carried out to optimize TC and CIP removal using bimetallic (SS-Fe/Cu) nanocomposite under different operating conditions, including pH, contact time, stirring speed, initial pollutant concentration, and nanocomposite dose. Several experiments were conducted. First, 50 mL of pollutant solution with a concentration of 50 mg/L was put into a 250 mL conical flask. Next, 1 g of nanocomposite was added to each 50 mL of pollutant solution. An orbital shaker set to 200 rpm was used to agitate this mixture for 3 h. Following processing, Whatman filter paper No. 1 was used to filter the pollutant solution and remove any remaining nanoparticles. The double-beam UV-visible spectrophotometer was used to quantify the residual antibiotics, taking into account the wavelengths of 275 nm for CIP and 357 nm for TC. The batch experiments were performed at different values of parameters, contact time (0-180 min), pH (2-12), initial pollutant concentration (10-50 mg/L), stirring speed (0-250 rpm), and SS-Fe/Cu dosage (0.05-1.2 mg/50 mL). The removal percentage (R%) and quantity of pollutants on the solid phase (q_e) were calculated using Eqs. 1 and 2, respectively [36, 37].

$$R\% = \frac{C_O - C_e}{C_O} * 100 \quad (1)$$

$$q_e = \frac{C_O - C_e}{m} V \quad (2)$$

Where V is the solution's volume in liters (L), m is the mass of the SS-Fe/Cu nanocomposite in grams (g), and C_o and C_e stand for the initial and equilibrium pollutant concentrations, respectively, in mg/L.

2.5. Adsorption isotherm models

Two specific isotherm models were examined to characterize the equilibrium correlation between the adsorbate concentrations at a given temperature in the liquid and solid phases [38]. These two models are the Langmuir and the Freundlich isotherm models:

* Langmuir isotherm: The Langmuir isotherm is based on the idea of homogeneous surfaces and monolayer adsorption that occurs only on the adsorbent's surface, which involves a limited number of active sites. Eqs. 3 and 4 represent the nonlinear and linearized forms of the Langmuir isotherm, respectively, as follows:

$$q_e = \frac{K_L q_m C_e}{1 + K_L C_e} \quad (3)$$

$$\frac{1}{q_e} = \frac{1}{q_m} + \frac{1}{q_m K_L} \frac{1}{C_e} \quad (4)$$

Where: q_e is the mass of the solute adsorbed per unit mass of the adsorbent at equilibrium (mg/g), q_m is the maximum adsorption capacity (mg/g), K_L is the Langmuir constant, and C_e is the concentration of contaminants in the bulk solution at equilibrium (mg/L).

* Freundlich isotherm: Unlike the Langmuir model, the Freundlich isotherm model is for heterogeneous surfaces and multi-layer adsorption. The following Eqs. 5 and 6 express their non-linear and linearized forms, respectively.

$$q_e = K_F C_e^{\frac{1}{n}} I \quad (5)$$

$$ln\, q_e = ln\, K_F + \frac{1}{n} ln\, C_e \quad (6)$$

Where: K_F represents the Freundlich coefficient ((mg/g) $(L/mg)^{1/n}$), while n is an empirical value that reflects the intensity of adsorption [39, 40].

2.6. Adsorption Kinetics

An understanding of the solute's transfer rate from the aqueous to the solid phase is necessary to design an effective adsorption method [41]. The following two models are employed to determine this rate:

* Pseudo-first order: Based on the assumption that the sorption process follows first-order kinetics, this model makes it possible to calculate the sorption rate using Eq.7.

$$\frac{dq_t}{dt} = K_1 (q_e - q_t) \quad (7)$$

The linearized form of the previous equation is given by Eq. 8.

$$ln(q_e - q_t) = ln\, q_e - K_1 t \quad (8)$$

* Pseudo-second order: According to this model, the sorption process follows second-order kinetics, which can be mathematically represented by Eq. 9 and its linearized form, Eq. 10.

$$\frac{dq_t}{dt} = K_2 (q_e - q_t)^2 \quad (9)$$

$$\frac{t}{q_t} = \frac{1}{K_2 {q_e}^2} + \frac{t}{q_e} \quad (10)$$

Where: dq_t/dt represents the adsorption rate, q_e is the sorption capacity at equilibrium (mg/g), q_t represent the amount of solute adsorbed at time t (mg/g), K_1 and K_2 denotes the pseudo-first and second-order rate constants, respectively [42, 43].

2.7. Thermodynamic

Thermodynamic characteristics serve as indicators of the process's favorability and offer important insights into the nature and mechanism of the adsorption process [44]. The thermodynamic adsorption parameters may be easily computed because the adsorption process is temperature-dependent [45]. The thermodynamic parameters are enthalpy change (ΔH^o), entropy change (ΔS^o), and Gibbs free energy change (ΔG^o). Eq. 11 was used to determine the Gibbs free energy change.

$$\Delta G^o = -RT\, ln\, K_c \quad (11)$$

and Eq. 12 is applied to calculate the value of K_c.

$$K_c = \frac{q_e}{C_e} \quad (12)$$

The three thermodynamic parameters have been combined in a single correlation (Eq. 13), which is then substituted in Eq. 11, yielding Eq. 14 [42, 43], which can be employed to determine the values of ΔH^o and ΔS^o by the linear plot of $1/T$ verses $\ln K_c$.

$$\Delta G^o = \Delta H^o - T\Delta S^o \quad (13)$$

$$ln\, K_c = \frac{\Delta S^o}{R} - \frac{\Delta H^o}{RT} \quad (14)$$

3- Results and discussion

3.1. Characterization of synthesized SS-Fe/Cu nanocomposite

3.1.1. XRD analysis

Fig. 2 shows the XRD spectral data for sand before and after coating with Fe/Cu nanoparticles. For silica sand, the main peak at 26.912 degrees corresponds to quartz (SiO_2), the primary component of silica sand. This is a well-known sharp peak indicative of crystalline quartz. The intensity of this peak (~26.912) significantly decreases after coating with Fe/Cu nanoparticles. The formation of Fe and Cu nanoparticles on the sand surface is confirmed by the diffraction peaks at 2θ= 46.2201 and 50.9527 [46]. These peaks indicate new structural features on the sand surface, suggesting that the formerly inert sand has become more reactive [47]. Additionally, the XRD pattern of the SS–Fe/Cu nanocomposite shows diffraction peaks at 2θ ≈ 36.6° and 37°, corresponding to FeO and CuO, respectively. These results imply the formation of iron oxide and copper oxide phases following alkaline treatment of Fe^{3+} and Cu^{2+} salts. These oxides are known to provide active surface sites for adsorbing organic contaminants, especially antibiotics such as TC and CIP, which possess multiple functional groups capable of complexation and hydrogen bonding. Their presence likely improves the material's adsorption capacity through electrostatic attraction, coordination bonds, and π–π interactions.

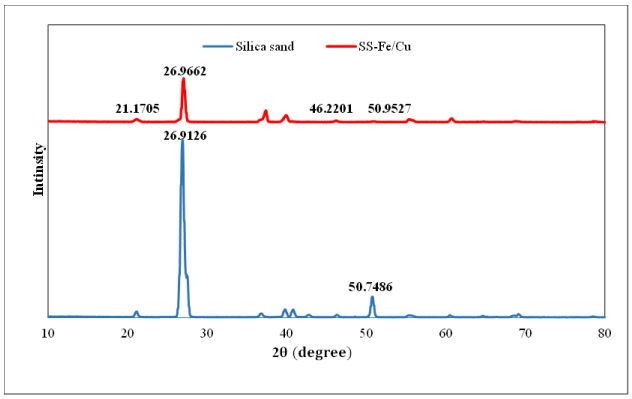

Fig. 2. XRD Pattern for Silica sand and SS-Fe/Cu nanocomposite

3.1.2. FTIR analysis

Fig. 3 presents the spectral data of SS–Fe/Cu nanocomposite performed using Fourier Transform Infrared (FTIR) spectroscopy, spanning from 400 to 4000 cm^{-1} to detect the chemical bonds and functional groups that enable the binding and removal of pollutants. FT-IR spectra revealed strong peaks typical of Si–O–Si asymmetric stretching for silica at 1080.14 cm^{-1}, which were shifted in Fig. 3 (b, c, and d), indicating the covalent

bonding of sand with SS-Fe/Cu nanoparticles. Conocarpus leaf extract typically contains polyphenols, flavonoids, and antioxidants represented by O-H, C-H, and C=O functional groups, which can be shown at 3414, 2918.3, and 1681.93 cm^{-1} peaks. This result is in line with earlier research that used pomegranate peel extract to create metal nanoparticles [36]. Peaks observed between 600–400 cm^{-1} (specifically at 474, 464, and 484 cm^{-1}) correspond to Fe–O and Cu–O stretching, confirming the incorporation of Fe and Cu nanoparticles. Moreover, the FTIR spectra confirms TC and CIP removal, the peaks of 1616.3 and 1680 cm^{-1} for C=O are mainly due to functional groups in tetracycline and ciprofloxacin, demonstrating the existence of such pollutants that have been adsorbed to the surface of nanoparticles. When certain wavenumber peaks shift, the affinity between the functional sets in the target pollutants and those on the sorbent surface increases even further [48].

3.1.3. FE-SEM/EDS analysis

As seen in Fig. 4 (a, b, c, and d), the surface morphology of silica sand and the synthesized nanoparticles, both before and after the sorption of TC and CIP, was obtained using FE-SEM analysis. In Fig. 4 (a), the surface of silica sand appears smooth with a limited number of active sites. Significant variations in the sand's surface morphology were noticed in Fig. 4 (b), which is considered an indication of the nanocomposite's successful loading on the silica sand's surface. The majority of these nanoparticles exhibited a semi-spherical morphology, and the surface was rough and granular. In nanoparticle synthesis, the spherical shape is preferred because of its high surface area-to-volume ratio. Fig. 4 (c, d) displayed a more intricate structure than Fig. 4 (b) with agglomerated and obscured surface features, suggesting a successful binding between the nanocomposite surface and the two contaminants. The results of the EDS analysis verified that silica sand's surface included Fe and Cu nanoparticles. Additionally, the presence of carbon (C) and nitrogen (N) in the elemental analysis confirmed that tetracycline and ciprofloxacin were effectively loaded onto the surface of the nanocomposite as organic contaminants.

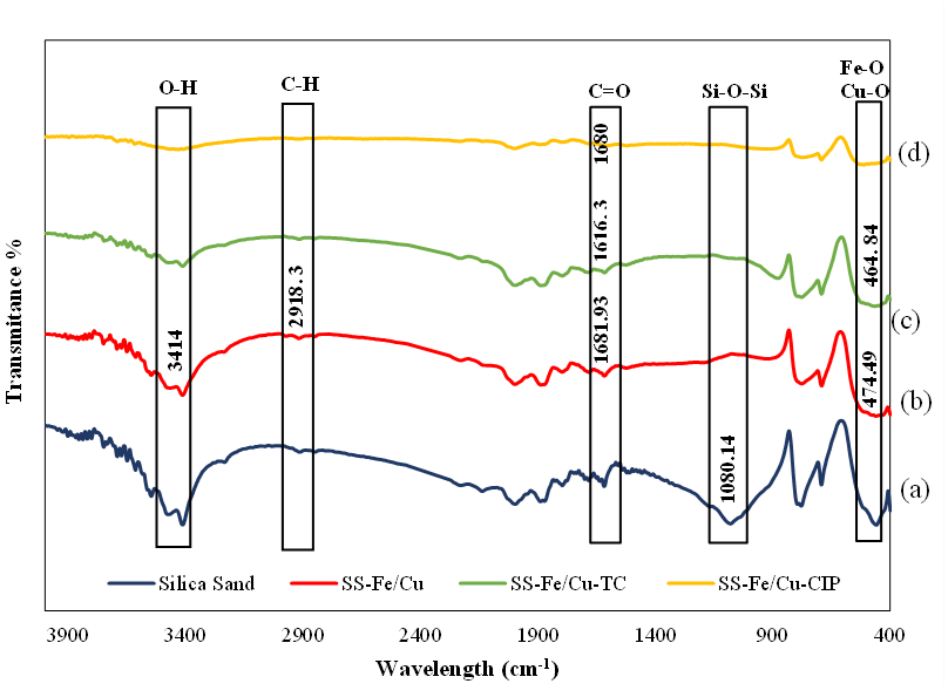

Fig. 3. FTIR data for (a) Silica sand, (b) SS-Fe/Cu nanocomposite, (c) SS-Fe/Cu-TC, and (d) SS-Fe/Cu-CIP

3.1.4. TEM analysis

Fig. 5 (a, b) displays TEM results of silica sand and SS-Fe/Cu nanocomposite. When looking at Fig. 5 (a), it is clear that the sand particles appear as a uniform mass free of small pieces, indicating that the sand surface is not coated with additional materials. The appearance of small, irregular fragments, on the other hand, is depicted in Fig. 5 (b), which differs significantly from Fig. 5 (a). The presence of these fragments indicates that there are nanoparticles (Fe, Cu) on the silica sand surface, suggesting that the nanoparticles were successfully deposited on the sand surface. The nanoparticles appear to be spherical to slightly irregular in shape, with different sizes. The particles are generally well-dispersed, likely due to magnetic or electrostatic interactions. The nanoscale size and distribution of the metallic particles enhance the surface reactivity and provide abundant active sites for contaminants adsorption, contributing to the improved performance observed in subsequent adsorption experiments.

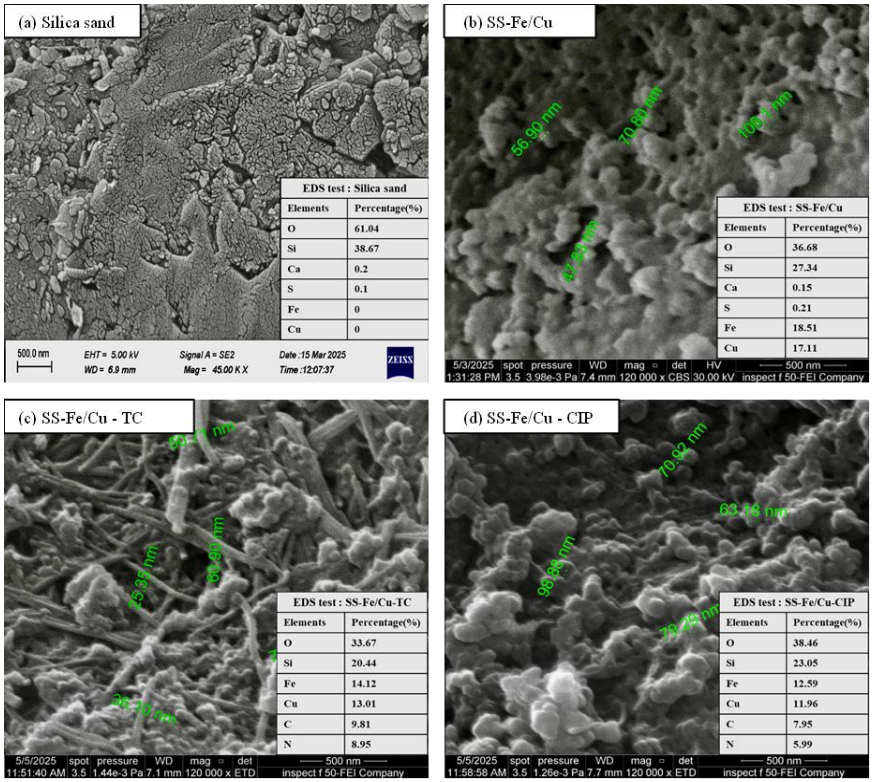

Fig. 4. FE-SEM/EDS test for (a) Silica sand, (b) SS-Fe/Cu nanocomposite, (c) SS-Fe/Cu-TC, and (d) SS-Fe/Cu-CIP

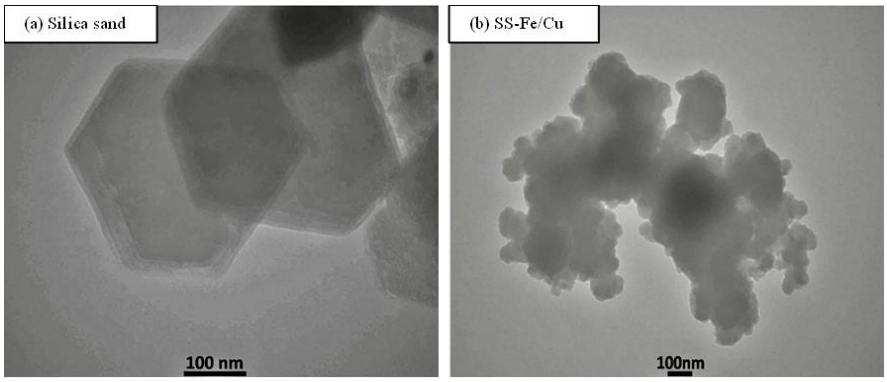

Fig. 5. TEM images for (a) Silica sand and (b) SS-Fe/Cu nanocomposite

3.1.5. BET analysis

The surface properties of silica sand and SS-Fe/Cu nanocomposite were determined by BET analysis. The nitrogen adsorption-desorption isotherms and corresponding BJH pore size distribution are shown in Fig. 6 (a, b), and the results are summarized in Table 2. Immobilization of Fe/Cu NPs on the silica sand results in an augmentation of both the total surface area of the sand, increasing from 12.115 m^2/g to 15.472 m^2/g, and the pore volume, increasing from 0.01766 cm^3/g to 0.0283 cm^3/g, which promotes a more uniform distribution and a higher adsorption capacity for TC and CIP.

Fig. 6 (a) illustrates that an increase in gas adsorption per unit mass of the adsorbent at a specific relative pressure indicates that the synthesized nanoparticles possess a greater ability to adsorb gas. This conclusion is supported by the observation that nitrogen adsorption for sand particles was significantly enhanced after coating with nanoparticles [49]. The pore size distributions of silica sand and SS-Fe/Cu nanocomposite were determined using the BJH method. Fig. 6 (b) displays the curves that show the distribution of pore sizes. The curves displayed a wide spread of mesopores in the sand sample, while the SS-Fe/Cu nanocomposite sample showed comparable peaks.

3.1.6. TGA analysis

Fig. 7 shows the thermogravimetric analysis of the prepared nanocomposite material. The TGA curve exhibits a total weight loss of about 48% by 900 °C. The decomposition can be divided into three stages. In the first stage (ambient to about 190 °C), the mass loss is about 34%. This loss is attributed to the removal of a highly volatile component, since nZVI particles are often highly hygroscopic and tend to adsorb large amounts of water due to their high surface area during the chemical

synthesis and washing steps. In stage 2(190 to 450 ºC), the curve slope decreases, indicating a slower but continuous mass loss from ≈34% to ≈42% (an additional ≈8% loss). This stage typically corresponds to the thermal decomposition or combustion of organic stabilizing agents (e.g., polymers, surfactants, or plant extracts) used to prevent the Fe/Cu nanoparticles from aggregating during synthesis. In the third stage (450 ºC to 900 ºC), extremely slow mass loss occurs, indicating the total loss of about 49% eventually flattens out to a plateau.

3.1.7. DSC analysis

Fig. 8 shows the DSC curve, which confirms that the SS-Fe/Cu nanocomposite is thermally stable up to approximately 450 ºC. Above this temperature, the material undergoes a major, rapid, and highly exothermic oxidation reaction, which limits its long-term stability and maximum operating temperature in an oxygen-containing environment. The stability observed up to 450 ºC is often a benefit of supporting the nanoparticles on a thermally inert material like silica sand. The thermally stable behavior up to 450 °C ensures that the nanocomposite will not degrade during storage or handling. Furthermore, the pronounced exothermic reaction above 450 °C highlights the upper thermal limit, which is critical for designing processes that involve high temperatures or oxidative environments. Overall, the DSC results confirm that the silica-supported bimetallic nanoparticles combine both high thermal stability and practical applicability in aqueous pollutant removal.

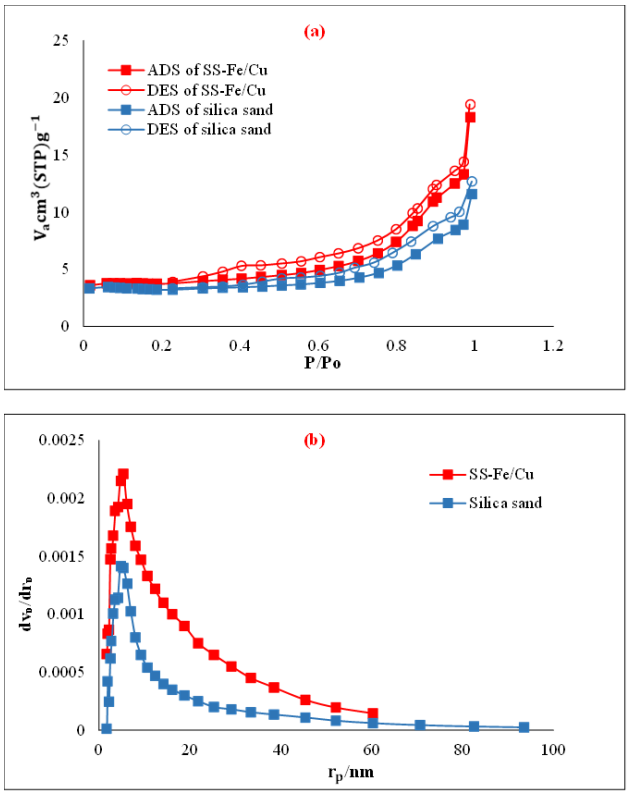

Fig. 6. BET analysis, (a) nitrogen adsorption-desorption isotherms, (b) BJH pore size distribution for silica sand and SS-Fe/Cu nanocomposite

Table 2. BET analysis results for silica sand and SS-Fe/Cu nanocomposite

Material	V_m [cm^3(STP) g^{-1}]	$A_{s,BET}$ [m^2 g^{-1}]	Total pore volume [cm^3 g^{-1}]	Ave. pore diameter [nm]	V_p [cm^3 g^{-1}]	A_p [m^2 g^{-1}]
Silica Sand	2.7834	12.115	0.01766	5.8318	0.013836	2.7521
SS-Fe/Cu	3.5548	15.472	0.0283	7.3164	0.024869	5.9058

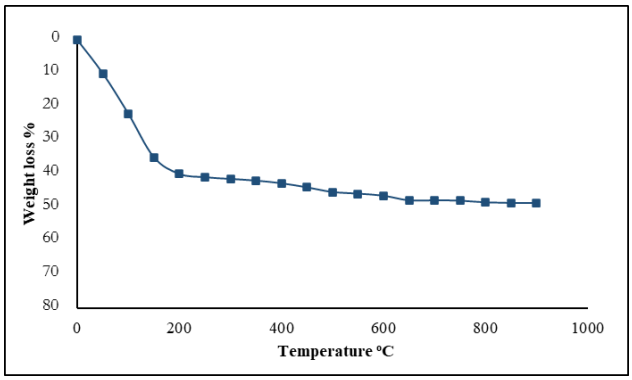

Fig. 7. TGA graph of SS-Fe/Cu nanocomposite prepared at optimized conditions

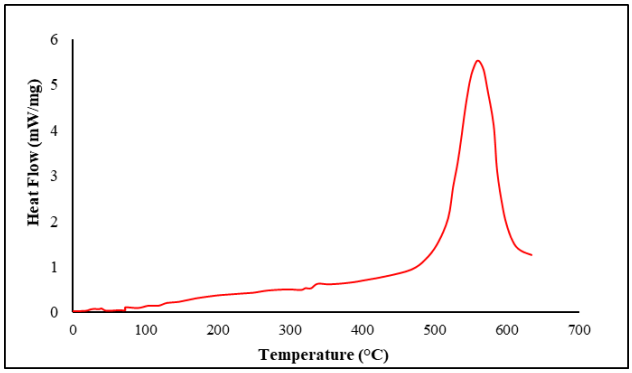

Fig. 8. DSC curve of SS-Fe/Cu nanocomposite at heating rate 10 ºC/min

3.2. Effect of operational factors

3.2.1. Contact time

To find the optimal length to attain the highest removal effectiveness of the designated contaminants (TC and CIP), the equilibrium time must be established. This study examined the effect of contact time on the removal of TC and CIP over a range of 0–180 min. According to the results, the availability of active sites caused the removal of the pollutants to increase rapidly with time. The optimum operating time for the removal of both pollutants was 90 min, with removal percentages of 45% and 30% for TC and CIP, respectively, as illustrated in Fig. 9 (a). The removal declined significantly after 90 min, and there was no discernible change in the removal percentage due to the saturation and depletion of active sites on the SS-Fe/Cu nanocomposite until it reached equilibrium removal. Thus, 90 minutes is the ideal contact time needed to reach equilibrium to remove TC and CIP.

3.2.2. Initial solution's pH

The most crucial parameter in the investigation of TC and CIP degradation is the solution's initial pH; the range of pH studied in the experiments was 2-12, and the initial pH of TC and CIP solutions was 4 and 6, respectively, and it was adjusted across the range of 2 to 12 using 1 M NaOH and 1 M HCl solutions. As shown in Fig. 9 (b), the results demonstrated that the optimum pH for TC removal was 11, with a maximum removal efficiency of 60%. This indicates that the removal increases steadily as pH rises, and this pattern is consistent with a previous investigation [41]. This may be attributed to changes in surface charge and protonation of the nanocomposite, which reduce electrostatic repulsion between the pollutants and the adsorbent [50]. Conversely, the optimum pH for the removal of CIP was 7, with a maximum removal efficiency of 30%. This behavior agrees with previous studies, as reported in Liu, et al. [51]. As the pH value increases from 2 to 7, the removal percentage also increases because of the attraction between CIP and the sorbent functional sites. However, as the pH value increases beyond 7, the removal percentage declines because of the ionisation of the hydroxyl group [52, 53].

In general, the adsorption behavior of antibiotics is highly pH-dependent due to their amphoteric nature. At low pH values, the antibiotic molecules are predominantly in their protonated (cationic) form, which may result in electrostatic repulsion if the adsorbent surface is also positively charged (e.g., $Fe–OH_2^+$ or $Cu–OH_2^+$ groups). At intermediate to high pH values, the antibiotics may exist in zwitterionic or anionic forms, increasing the likelihood of electrostatic attraction to positively charged surface sites or enabling hydrogen bonding and surface complexation. Although the point of zero charge (pHpzc) of the SS–Fe/Cu nanocomposite was not measured directly, the observed adsorption trends are consistent with the general behavior of silica and metal oxide surfaces, which become negatively charged at higher pH. These interactions collectively explain the variation in adsorption efficiency with pH.

3.2.3. Agitation speed

The influence of stirring speed on the antibiotic's removal has been examined across a spectrum of 0 to 250 rpm. In the absence of agitation, approximately 15% of TC and 8% of CIP were removed. The natural settling process or the poor interactions between the contaminants and the sorbent surface could be the cause of this initial removal. As the rotational speed increases, the efficiency of removal also rises (60% for TC & 30% for CIP), peaking at 200 rpm [54]. However, as depicted in Fig. 9 (c), increasing the speed to 250 rpm did not result in a significant improvement in removal rates. Therefore, 200 rpm was chosen as the best speed to achieve a higher removal percentage. Enhanced agitation speeds facilitate a better distribution on the surface of the sorbent (SS-Fe/Cu nanocomposite). Thus, these observations can be explained by increasing the contact between the sorbate solution and the active sites [55].

3.2.4. Pollutant's initial concentration

To investigate the effects of different initial concentrations (C_o) of TC and CIP on the removal percentage, more experiments were conducted. Fig. 9 (d) illustrates the adsorption rates of TC and CIP onto the SS-Fe/Cu nanocomposite across various initial concentrations (10, 20, 30, 40, and 50 ppm). The graph indicates a significant decrease in the removal efficiency of both contaminants as the initial concentration rises. This decrease in removal rates is related to the contaminating particles' quick saturation of the active sites on the produced nanoparticles at increasing concentrations, leading to diminished nanoparticle effectiveness [56, 57]. As a result, a 10 mg/L initial concentration was determined to be optimal, achieving maximum removal rates of 75% for TC and 65% for CIP.

3.2.5. SS-Fe/Cu dosage

Through a series of tests using different nanocomposite amounts ranging from 0.05 to 1.2 g/50 mL, the dependence of TC and CIP removal on the dosages of SS-Fe/Cu was investigated (Fig. 9 (e)). According to earlier parameter investigations, only 75% of TC and 65% of CIP were eliminated using only 0.3 g/50 mL of synthesized nanoparticles. Hence, a clear improvement in the removal effectiveness of both pollutants was observed with an increase in dosage, achieving optimum removal at 1g/50 mL with a removal percentage of 93% for TC and 85% for CIP. This rise is brought on by the larger dosage of adsorbent, which makes more accessible sorption sites available [58, 59]. However, after a certain dosage (1 g/50 mL), the adsorption process hits a saturation limit, meaning that adding more sorbent does not appreciably increase the number of active sites available for pollutant attachment [23].

3.3. Adsorption isotherm

As stated earlier, two models, the Langmuir and the Freundlich models, are employed to analyze the equilibrium results from the sorption tests concerning the interaction between SS-Fe/Cu nanocomposite and TC and CIP. Adsorption isotherm studies were conducted at a temperature of 298 K. A comparison of these models with the experimental data is given in Fig. 10. The parameters related to them are summarized in Table 3. The Freundlich model provided the best fit for TC and CIP adsorption onto the SS-Fe/Cu nanocomposite, as evidenced by higher R^2 values of 0.976 and 0.9587 for TC and CIP, respectively, which may imply that the Freundlich model is more suitable for representing the adsorption process and can fit the data better than the Langmuir model. It can therefore be assumed that the adsorption of both TC and CIP takes place in a multilayer molecular structure on the surface of the SS-Fe/Cu

nanocomposite. Although non-linear regression methods can sometimes offer improved accuracy in parameter estimation, the linearized versions remain widely used in adsorption studies due to their simplicity, ease of parameter extraction, and comparability with many published works, providing a valid and reliable way to assess adsorption behavior. Therefore, the linear forms of the Langmuir and the Freundlich models were employed in this study.

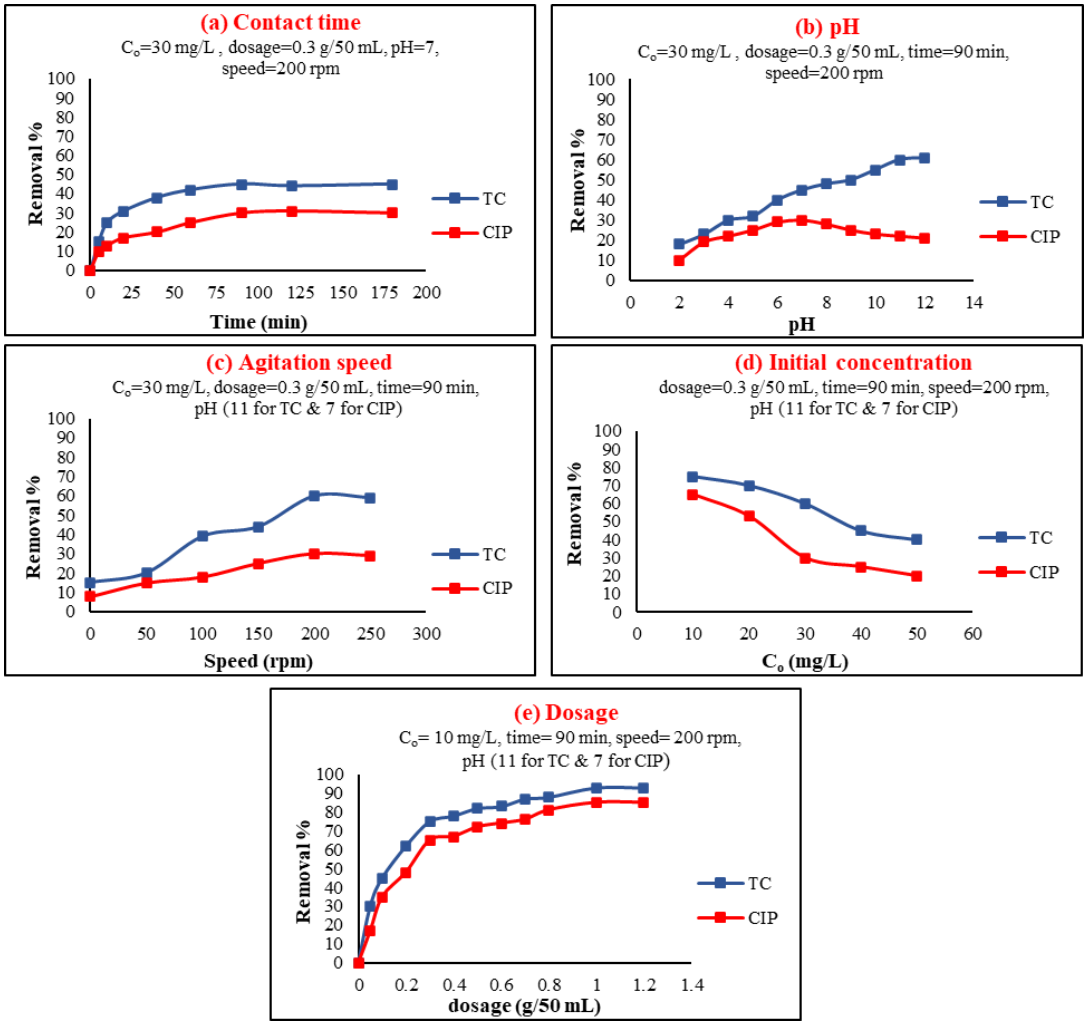

Fig. 9. Removal percentage of TC and CIP under various operational conditions, (a) Contact time, (b) pH, (c) Agitation speed, (d) Initial concentration, and (e) Sorbent Dosage

3.4. Adsorption kinetics

The models were determined by assessing the experimental data alongside their linearized versions. As illustrated in Fig. 11 and detailed in Table 4, the sorption of TC and CIP likely follows second-order kinetics, irrespective of the R^2 values; the modeled q_e values were more aligned with the experimental results. The experimental measurements for q_e stand at 0.435 mg/g for TC and 0.411 mg/g for CIP, closely matching the calculated q_e values. Furthermore, this model produced the highest R^2 values for both contaminants, reinforcing the notion that their sorption is predominantly second-order. The findings suggest that the uptake of both TC and CIP on SS-Fe/Cu nanocomposite primarily occurred via chemisorption or ion exchange mechanisms. These results are consistent with those of other researchers, including [60, 61].

3.5. Thermodynamic

As illustrated in Fig. 12, the elimination of TC and CIP using SS-Fe/Cu nanocomposite yielded all thermodynamic data (ΔG°, ΔH°, and ΔS°) at temperatures ranging from 288 to 338 K. With a positive value of enthalpy (ΔH° = 15258.684 J/mol) and entropy (ΔS° = 29.173 J/mol.K), the thermodynamic characteristics obtained for the adsorption of TC suggest that the process is endothermic and that there is more randomness at the solid–solution interface during adsorption. However, at the temperature range (Table 5), the computed Gibbs free energy change (ΔG°) values were positive, suggesting that the process is non-spontaneous under the experimental conditions. The process's spontaneity is very

temperature-dependent because both ΔH° and ΔS° are positive. Raising the temperature may cause the ΔG° values to shift negative, which would make the process spontaneous. Consequently, it is proposed that operating at higher temperatures could improve the thermodynamic favorability of TC adsorption in this system [62, 63].

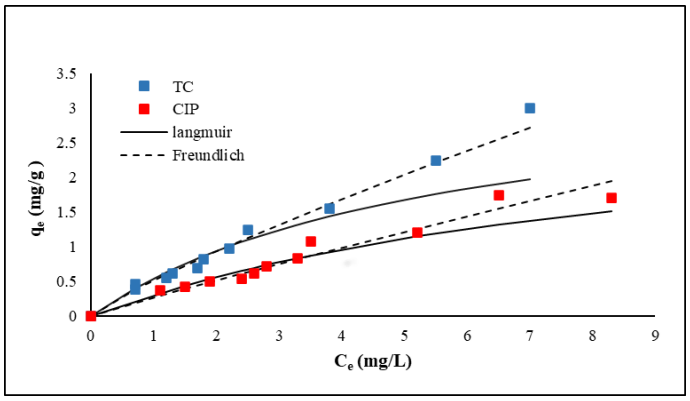

Fig. 10. Isotherm models and experimental data for TC and CIP adsorption

Table 3. Sorption isotherm model constants with determination coefficients for the sorption of TC and CIP using SS-Fe/Cu nanocomposite

Model	Parameter	TC	CIP
Langmuir model	(mg/g)q_m	3.539	3.297
	(L/mg)K_L	0.1815	0.103
	R^2	0.936	0.935
Freundlich model	(mg/g) $(L/mg)^{1/n}K_F$	0.517	0.269
	n	1.172	1.068
	R^2	0.976	0.9587

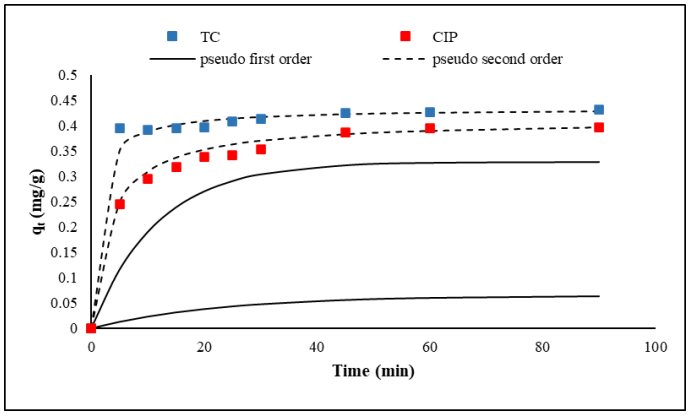

Fig. 11. Kinetics models and experimental data for TC and CIP adsorption

Table 4. Sorption kinetic models constants with determination coefficients for the sorption of TC and CIP using SS-Fe/Cu nanocomposite

Model	Parameter	TC	CIP
Experimental	(mg/g)q_e	0.432	0.396
Pseudo-first order	(mg/g)q_e	0.064	0.329
	(1/min)K_1	0.044	0.086
	R^2	0.949	0.958
Pseudo-second order	(mg/g)q_e	0.435	0.411
	(g/mg min)K_2	1.884	0.733
	R^2	0.999	0.996

Unlike TC, the CIP adsorption thermodynamic characteristics show that the process is exothermic, as evidenced by the negative ΔH° value (- 47733.99 J/mol) and ΔS° value (- 156.053 J/mol.K), which reflect a reduction in randomization at the solid/solution interface during the adsorption process. As the temperature rises (Table 5), the Gibbs free energy change (ΔG°) becomes more positive, suggesting that the process is spontaneous at lower temperatures but tends to become non-spontaneous at higher ones. In lower temperature ranges, where the exothermic nature predominates, and entropy loss is less penalizing, this implies that adsorption is thermodynamically preferred [64, 65].

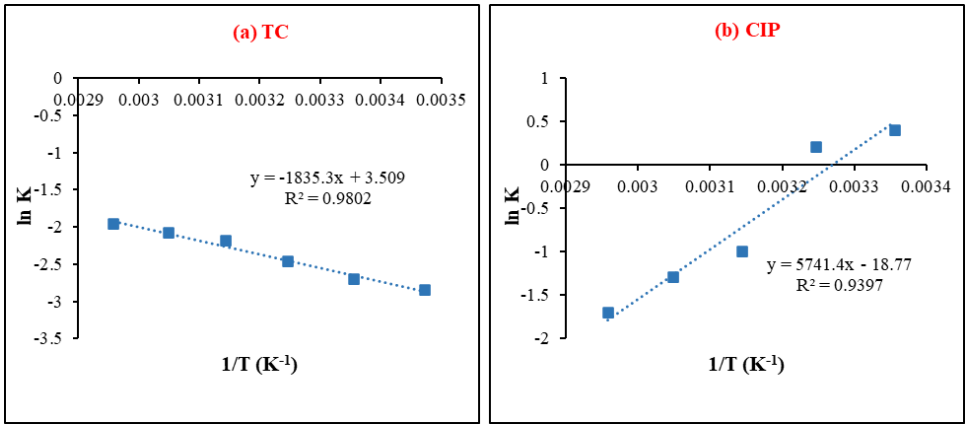

Fig. 12. Thermodynamic study for the adsorption of (a) TC and (b) CIP using SS-Fe/Cu nanocomposite

Table 5. Values of ΔG° for the sorption of TC and CIP using SS-Fe/Cu nanocomposite at different temperatures

T(K)		288	298	308	318	328	338
ΔG°	TC	6856.86	6565.13	6273.4	5981.67	5689.94	5398.21
J/mol	CIP	-2790.7	-1230.2	330.325	1890.86	3451.38	5011.91

3.6. Reusability of SS-Fe/Cu nanocomposite

To verify the applicability of the adsorbent in industrial practice and the possibility of being used multiple times, the reusability of the adsorbent must be investigated. Repeatedly, the newly prepared TC and CIP solutions were treated with the previously used SS-Fe/Cu nanocomposite to evaluate their reusability in a batch process. The nanocomposite was washed with distilled water, dried in an oven at 70℃, and reused in multiple consecutive cycles. The removal efficiencies were 93% for TC and 85% for CIP for the first cycle. During the increase in reuse cycles, a successive decrease in removal efficiency was observed, as illustrated in Fig. 13. This behavior likely results from active site saturation or surface property changes after repeated use. This reduction is possibly worsened by accumulated contaminants hindering active site accessibility and electrochemical variations altering reaction kinetics. Low leaching after 5 cycles indicated that the Fe/Cu nanoparticles remained firmly bound and structurally intact during reuse. Therefore, this evidence indicates that the preparation of Fe/Cu nanoparticles on silica sand can be carried out in an economically feasible way, along with environmental friendliness.

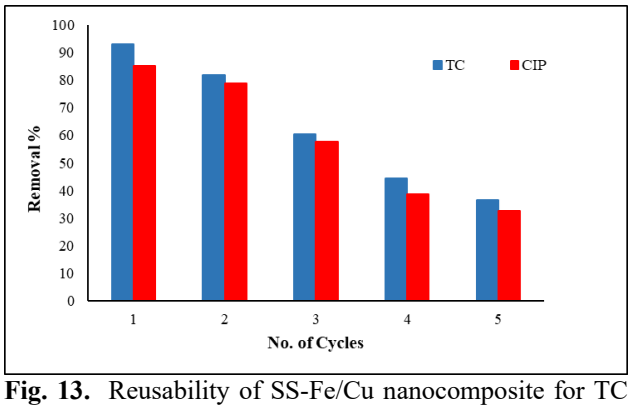

Fig. 13. Reusability of SS-Fe/Cu nanocomposite for TC and CIP removal

4- Conclusion

This study explored the utilization of Conocarpus leaf extract for the green synthesis of Fe/Cu bimetallic nanoparticles supported on silica sand to form the SS-Fe/Cu nanocomposite. Understanding the role of green extract in the formation of the SS-Fe/Cu nanocomposite and providing a scientific explanation for the removal mechanism were made possible by the use of strong and advanced characterization techniques, such as XRD, FTIR, BET, FE-SEM, EDS, TEM, TGA, and DSC, to ascertain the physical properties and chemical structure. In batch experiments and under optimal conditions (90 min contact time, 10 mg/L initial pollutant concentration, pH 11 for TC and 7 for CIP, 200 rpm agitation, and 1 g/50 mL nanocomposite dosage), SS-Fe/Cu nanocomposite removed TC (93%) more effectively than CIP (85%). Isotherm analyses revealed that the adsorption of both pollutants adhered to the Freundlich model, suggesting multilayer adsorption. Kinetic analysis revealed that chemisorption was the primary mechanism for both TC and CIP, and the pseudo-second-order model best described the experimental data. Thermodynamic analysis showed that TC adsorption was endothermic, non-spontaneous, entropy-driven (positive ΔS°), while CIP adsorption was exothermic, spontaneous, accompanied by a decrease in randomness (negative ΔS°). Because of its high efficiency and reactivity, these results indicate that the green-synthesised SS-Fe/Cu nanocomposite is a potential material for water treatment and environmental remediation. Future work can focus on improving the concepts of sustainable development by utilizing more affordable and environmentally friendly by-product wastes as green antioxidants instead of hazardous chemicals. In addition, the use of actual wastewater samples is recommended to further evaluate the efficiency of the prepared adsorbent under realistic conditions. Moreover, extending this study to investigate the simultaneous removal of both contaminants in binary systems and applying the developed adsorbent in a

continuous flow system is suggested to better simulate practical wastewater treatment applications.

References

[1] Z. T. Abd Ali, "Green synthesis of graphene-coated sand (GCS) using low-grade dates for evaluation and modeling of the pH-dependent permeable barrier for remediation of groundwater contaminated with copper," *Separation Science and Technology*, vol. 56, no. 1, pp. 14–25, Jan. 2021, https://doi.org/10.1080/01496395.2019.1708937

[2] S. M. Ibrahim, "Removal of acidic dye from aqueous solution using surfactant modified bentonite (organoclay): batch and kinetic study," *Journal of Engineering*, vol. 26, no. 5, pp. 64–81, 2020, https://doi.org/10.31026/j.eng.2020.05.05

[3] M. R. Shaibur, F. K. S. Tanzia, S. Nishi, N. Nahar, S. Parvin, and T. A. Adjadeh, "Removal of Cr (VI) and Cu (II) from tannery effluent with water hyacinth and arum shoot powders: A study from Jashore, Bangladesh," *Journal of Hazardous Materials Advances*, vol. 7, p. 100102, Aug. 2022, https://doi.org/10.1016/j.hazadv.2022.100102

[4] A. A. H. Faisal, M. B. Abdul, K. Alaa, K. Mohammed, A. A. Ghfar, and M. B. A. Kareem, "Novel Sorbent of Sand Coated with Humic Acid - Iron Oxide Nanoparticles for Elimination of Copper and Cadmium Ions from Contaminated Water," *Journal of Polymers and the Environment*, vol. 29, no. 11, pp. 3618–3635, 2021, https://doi.org/10.1007/s10924-021-02132-3

[5] Z. Salari, R. Jalilzadeh Yengejeh, A. A. Babaei, L. Roomiani, and S. Sabzalipour, "Removal of Florfenicol Antibiotic from Aquaculture Effluent Using an Integrated Strategy of Advanced Oxidation and Moving Bed Biofilm Reactor (AOP/MBBR)," *Iranian Journal of Chemistry and Chemical Enineering,* vol. 43, no. 12, pp. 4288–4300, 2024, https://doi.org/10.30492/ijcce.2024.2024482.6488

[6] B. H. Graimed and Z. T. Abd Ali, "Green approach for the synthesis of graphene glass hybrid as a reactive barrier for remediation of groundwater contaminated with lead and tetracycline," *Environmental Nanotechnology, Monitoring & Management*, vol. 18, p. 100685, 2022, https://doi.org/10.1016/j.enmm.2022.100685

[7] Z. Jahani, N. Samadani Langeroodi, M. Khalafi, and A. Mokhtari, "Optimizing the Adsorption Conditions for Removing Tetracycline from Water Using ZnCl2-Activated Carbon Derived from Walnut Shell," *Iranian Journal of Chemistry and Chemical Enineering,* vol. 44, no. 10, 2025, https://doi.org/10.30492/ijcce.2025.2049827.6953

[8] S. Kaushal, A. Kumar, H. Bains, and P. P. Singh, "Photocatalytic degradation of tetracycline antibiotic and organic dyes using biogenic synthesized CuO/Fe2O3 nanocomposite: pathways and mechanism insights," *Environmental Science and Pollution Research,* vol. 30, no. 13, pp. 37092–37104, 2023, https://doi.org/10.21203/rs.3.rs-1743967/v2

[9] S. Liu *et al.*, "Ultra-high adsorption of tetracycline antibiotics on garlic skin-derived porous biomass carbon with high surface area," *New Journal of Chemistry*, vol. 44, no. 3, pp. 1097–1106, 2020, https://doi.org/10.1039/C9NJ05396D

[10] M. S. Ameer, M. A. Atiya, A. K. Hassan, A. M. Shakorfow, and N. Al Mhanna, "CuO/ZnO Nanocomposite Biosynthesis Approach Using Eucalyptus Leaves for Photodegradation of Tetracycline," *Al-Khwarizmi Engineering Journal*, vol. 20, no. 4, pp. 25–37, Dec. 2024, https://doi.org/10.22153/kej.2024.08.003

[11] W.-T. Jiang *et al.*, "Removal of ciprofloxacin from water by birnessite," *Journal of Hazardous Materials*, vol. 250–251, pp. 362–369, Apr. 2013, https://doi.org/10.1016/j.jhazmat.2013.02.015

[12] . Falyouna, I. Maamoun, K. Bensaida, Y. Sugihara, and O. Eljamal, "Removal of ciprofloxacin from aqueous solutions by nanoscale zerovalent iron-based materials: a mini review,", *Proceedings of International Exchange and Innovation Conference on Engineering & Sciences (IEICES),* 2020, https://doi.org/10.5109/4102485

[13] M. Yoosefian, S. Ahmadzadeh, M. Aghasi, and M. Dolatabadi, "Optimization of electrocoagulation process for efficient removal of ciprofloxacin antibiotic using iron electrode; kinetic and isotherm studies of adsorption," *Journal of Molecular Liquids*, vol. 225, pp. 544–553, Jan. 2017, https://doi.org/10.1016/j.molliq.2016.11.093

[14] Y. Jia, S. K. Khanal, H. Shu, H. Zhang, G.-H. Chen, and H. Lu, "Ciprofloxacin degradation in anaerobic sulfate-reducing bacteria (SRB) sludge system: Mechanism and pathways," *Water Research*, vol. 136, pp. 64–74, Jun. 2018, https://doi.org/10.1016/j.watres.2018.02.057

[15] A. El-Baz, I. Hendy, A. Dohdoh, and M. Srour, "Adsorption technique for pollutants removal; current new trends and future challenges – A Review," *The Egyptian International Journal of Engineering Sciences and Technology*, vol. 32, no. 1, pp. 1–24, Dec. 2020, https://doi.org/10.21608/eijest.2020.45536.1015

[16] Z. Othman, H. R. Mackey, and K. A. Mahmoud, "MXene/chitosan/lignosulfonate (MCL) nanocomposite for simultaneous removal of Co(II), Cr(VI), Cu(II), Ni(II) and Pb(II) heavy metals from wastewater," *2D Materials*, vol. 10, no. 2, p. 024004, Apr. 2023, https://doi.org/10.1088/2053-1583/acbd62

[17] R. Tahmasebpour and S. J. Peighambardoust, "Decontamination of tetracycline from aqueous solution using activated carbon/Fe3O4/ZIF-8 nanocomposite adsorbent," *Separation and Purification Technology*, vol. 343, p. 127188, 2024, https://doi.org/10.1016/j.seppur.2024.127188

[18] R. Foroutan, S. J. Peighambardoust, P. Latifi, A. Ahmadi, M. Alizadeh, and B. Ramavandi, "Carbon nanotubes/β-cyclodextrin/MnFe2O4 as a magnetic nanocomposite powder for tetracycline antibiotic decontamination from different aqueous environments," *Journal of Environmental Chemical Engineering*, vol. 9, no. 6, p. 106344, 2021, https://doi.org/10.1016/j.jece.2021.106344

[19] Y. Zhou *et al.*, "Applications of nanoscale zero-valent iron and its composites to the removal of antibiotics: a review," *Journal of Materials Science*, vol. 54, no. 19, pp. 12171–12188, Oct. 2019, https://doi.org/10.1007/s10853-019-03606-5

[20] N. A. Abdulhusain and Z. T. Abd Ali, "Green synthesis of sand-bimetallic Fe/Pb nanoparticles as an environmentally sustainable composite for ciprofloxacin and copper removal from aqueous solutions," *Desalination and Water Treatment*, vol. 287, pp. 155–166, 2023, https://doi.org/10.5004/dwt.2023.29361

[21] Y. He *et al.*, "Zeolite supported Fe/Ni bimetallic nanoparticles for simultaneous removal of nitrate and phosphate: Synergistic effect and mechanism," *Chemical Engineering Journal*, vol. 347, pp. 669–681, Sep. 2018, https://doi.org/10.1016/j.cej.2018.04.088

[22] M. Stefaniuk, P. Oleszczuk, and Y. S. Ok, "Review on nano zerovalent iron (nZVI): From synthesis to environmental applications," *Chemical Engineering Journal* vol. 287, pp. 618–632, Mar. 2016, https://doi.org/10.1016/j.cej.2015.11.046

[23] K. V. G. Ravikumar, G. Debayan, P. Mrudula, N. Chandrasekaran, and M. Amitava, "In situ formation of bimetallic FeNi nanoparticles on sand through green technology: Application for tetracycline removal," *Frontiers in Environmental Science*, vol. 14, no. 1, p. 16, Feb. 2020, https://doi.org/10.1007/s11783-019-1195-3

[24] Z. T. Abd Ali and N. A. Abdulhusain, "Containment of ciprofloxacin and copper in groundwater using nanocomposite prepared by the use of pomegranate peel extract: characterization, kinetic, and modeling study," *Desalination and Water Treatment*, vol. 315, pp. 327–341, 2023, https://doi.org/10.5004/dwt.2023.30139

[25] X. Wang, P. Huang, P. Zhang, C. Wang, F. He, and H. Sun, "Synthesis of stabilized zero-valent iron particles and role investigation of humic acid-Fex+ shell in Fenton-like reactions and surface stability control," *Journal of Hazardous Materials* , vol. 465, p. 133296, Mar. 2024, https://doi.org/10.1016/j.jhazmat.2023.133296

[26] H. S. Hadi and Z. T. Abd Ali, "Removal of amoxicillin and lead from aqueous solutions using immobilized nanoparticles: green synthesis, characterization, and kinetic study," *Desalination and Water Treatment*, vol. 312, pp. 119–131, 2023, https://doi.org/10.5004/dwt.2023.30064

[27] M. Can, "Green gold nanoparticles from plant-derived materials: an overview of the reaction synthesis types, conditions, and applications," *Reviews in Chemical Engineering,* vol. 36, no. 7, pp. 859–877, Oct. 2020, https://doi.org/10.1515/revce-2018-0051

[28] O. P. Bolade, A. B. Williams, and N. U. Benson, "Green synthesis of iron-based nanomaterials for environmental remediation: A review," *Environmental Nanotechnology, Monitoring & Management*, vol. 13, p. 100279, May 2020, https://doi.org/10.1016/j.enmm.2019.100279

[29] A. Mahmoud, M. M. El-Shafei, A. S. Mahmoud, M. Mostafa, and R. Peters, "Green synthesis of nano iron carbide: preparation, characterization and application for removal of phosphate from aqueous solutions," in *2018 AIChE Annual Meeting*, AIChE, 2018.

[30] H. S. Afifi, H. M. Al Marzooqi, M. J. Tabbaa, and A. A. Arran, "Phytochemicals of Conocarpus spp. as a Natural and Safe Source of Phenolic Compounds and Antioxidants," *Molecules*, vol. 26, no. 4, p. 1069, Feb. 2021, https://doi.org/10.3390/molecules26041069

[31] D. K. D. NASCIMENTO *et al.*, "Phytochemical Screening and Acute Toxicity of Aqueous Extract of Leaves of Conocarpus erectus Linnaeus in Swiss Albino Mice," *An. Acad. Bras. Cienc.*, vol. 88, no. 3, pp. 1431–1437, Aug. 2016, https://doi.org/10.1590/0001-3765201620150391

[32] M. Saadullah, B. A. Chaudary, and M. Uzair, "Antioxidant, Phytotoxic and Antiurease Activities, and Total Phenolic and Flavonoid Contents of *Conocarpus lancifolius* (Combretaceae)," *Tropical Journal of Pharmaceutical Research*, vol. 15, no. 3, p. 555, Apr. 2016, https://doi.org/10.4314/tjpr.v15i3.17

[33] J. A. A. Abdullah, M. Jiménez-Rosado, V. Perez-Puyana, A. Guerrero, and A. Romero, "Green Synthesis of FexOy Nanoparticles with Potential Antioxidant Properties," *Nanomaterials*, vol. 12, no. 14, p. 2449, Jul. 2022, https://doi.org/10.3390/nano12142449

[34] A. A. Naji and Z. T. Abd Ali, "Fabrication of immobilized magnetic nanoparticles for removal of cadmium and moxifloxacin from aqueous solutions using green approach: Batch and continuous study," *Case Studies in Chemical and Environmental Engineering*, vol. 9, p. 100771, 2024, https://doi.org/10.1016/j.cscee.2024.100771

[35] T. S. Merjan and Z. T. A. Ali, "Green synthesis of bimetallic and trimetallic nanoparticles on glass granules for lead removal," *Desalination and Water Treatment*, vol. 322, p. 101082, Apr. 2025, https://doi.org/10.1016/j.dwt.2025.101082

[36] N. Alaa Abdulhusain and Z. Tark Abd Ali, "Green approach for fabrication of sand-bimetallic (Fe/Pb) nanocomposite as reactive material for remediation of contaminated groundwater using permeable reactive barrier," *Alexandria Engineering Journal*, vol. 72, pp. 511–530, Jun. 2023, https://doi.org/10.1016/j.aej.2023.04.028

[37] A. Kareem Mohammed, I. M. M. Rashid, N. AL Sbani, and W. Wan Isaha, "Modification, Characterization of Tea Residue-derived Activated Carbon, and Ciprofloxacin Adsorption," *Al-Khwarizmi Engineering Journal*, vol. 20, no. 1, pp. 1–16, Mar. 2024, https://doi.org/10.22153/kej.2024.11.001

[38] Z. T. Abd Ali, "Combination of the artificial neural network and advection-dispersion equation for modeling of methylene blue dye removal from aqueous solution using olive stones as reactive bed," *Desalination and Water Treatment*, vol. 179, pp. 302–311, Mar. 2020, https://doi.org/10.5004/dwt.2020.25037

[39] I. M. Rashid, S. D. Salman, A. K. Mohammed, and Y. S. Mahdi, "Green Synthesis of Nickle Oxide Nanoparticles for Adsorption of Dyes," *Sains Malaysiana*, vol. 51, no. 2, pp. 533–546, Feb. 2022, https://doi.org/10.17576/jsm-2022-5102-17

[40] A. K. Mohammed, S. M. Saadoon, Z. T. Abd Ali, I. M. Rashid, and N. H. A. L. Sbani, "Removal of amoxicillin from contaminated water using modified bentonite as a reactive material," *Heliyon*, vol. 10, no. 3, 2024, https://doi.org/10.1016/j.heliyon.2024.e24916

[41] H. S. Hadi and Z. T. Abd Ali, "Green approach for the synthesis of nanocomposite used as reactive material to containment amoxicillin and lead in groundwater," *Case Studies in Chemical and Environmental Engineering*, vol. 9, p. 100707, Jun. 2024, https://doi.org/10.1016/j.cscee.2024.100707

[42] A. Adel Naji and Z. Tark Abd Ali, "A single-step method as a green approach to fabricate magnetite nanocomposite for removal of moxifloxacin and cadmium from aqueous solutions," *Environmental Nanotechnology, Monitoring & Management*, vol. 20, p. 100883, Dec. 2023, https://doi.org/10.1016/j.enmm.2023.100883

[43] S. Saadoon, A. K. Mohammed, Z. T. A. Ali, I. M. Rashid, W. N. R. W. Isahak, and M. Rahimnejad, "Removal of Diclofenac from Contaminated Water using Organoclay as Reactive Material," *Al-Khwarizmi Engineering Journal*, vol. 20, no. 2, pp. 1–13, Jun. 2024, https://doi.org/10.22153/kej.2024.12.001

[44] M. E. González-López, C. M. Laureano-Anzaldo, A. A. Pérez-Fonseca, M. Arellano, and J. R. Robledo-Ortíz, "A Critical Overview of Adsorption Models Linearization: Methodological and Statistical Inconsistencies," *Separation & Purification Reviews*, vol. 51, no. 3, pp. 358–372, Jul. 2022, https://doi.org/10.1080/15422119.2021.1951757

[45] S. K. Thaligari, V. C. Srivastava, and B. Prasad, "Adsorptive desulfurization by zinc-impregnated activated carbon: characterization, kinetics, isotherms, and thermodynamic modeling," *Clean Technologies and Environmental Policy*, vol. 18, no. 4, pp. 1021–1030, Apr. 2016, https://doi.org/10.1007/s10098-015-1090-y

[46] T. S. Soliman and S. A. Vshivkov, "Effect of Fe nanoparticles on the structure and optical properties of polyvinyl alcohol nanocomposite films," *Journal of Non-Crystalline Solids*, vol. 519, p. 119452, Sep. 2019, https://doi.org/10.1016/j.jnoncrysol.2019.05.028

[47] L. Du *et al.*, "Nitrogen–doped graphitized carbon shell encapsulated NiFe nanoparticles: A highly durable oxygen evolution catalyst," *Nano Energy*, vol. 39, pp. 245–252, Sep. 2017, https://doi.org/10.1016/j.nanoen.2017.07.006

[48] S. S. Shah, T. Sharma, B. A. Dar, and R. K. Bamezai, "Adsorptive removal of methyl orange dye from aqueous solution using populous leaves: Insights from kinetics, thermodynamics and computational studies," *Environmental Chemistry and Ecotoxicology*, vol. 3, pp. 172–181, 2021, https://doi.org/10.1016/j.enceco.2021.05.002

[49] T. D. Bennett, F.-X. Coudert, S. L. James, and A. I. Cooper, "The changing state of porous materials," *Nature Materials.*, vol. 20, no. 9, pp. 1179–1187, Sep. 2021, https://doi.org/10.1038/s41563-021-00957-w

[50] A. H. Sulaymon, A. A. H. Faisal, and Z. T. Abd Ali, "Performance of granular dead anaerobic sludge as permeable reactive barrier for containment of lead from contaminated groundwater," *Desalination and Water Treatment*, vol. 56, no. 2, pp. 327–337, Oct. 2015, https://doi.org/10.1080/19443994.2014.942376

[51] J. Liu, Y. Du, W. Sun, Q. Chang, and C. Peng, "A granular adsorbent-supported Fe/Ni nanoparticles activating persulfate system for simultaneous adsorption and degradation of ciprofloxacin," *Chinese Journal of Chemical Engineering*, vol. 28, no. 4, pp. 1077–1084, Apr. 2020, https://doi.org/10.1016/j.cjche.2019.12.019

[52] D. Wang, J. Li, Z. Xu, Y. Zhu, and G. Chen, "Preparation of novel flower-like BiVO4/Bi2Ti2O7/Fe3O4 for simultaneous removal of tetracycline and Cu2+: Adsorption and photocatalytic mechanisms," *Journal of Colloid and Interface Science*, vol. 533, pp. 344–357, Jan. 2019, https://doi.org/10.1016/j.jcis.2018.08.089

[53] Z. T. Abd Ali, H. J. Khadim, and M. A. Ibrahim, "Simulation of the remediation of groundwater contaminated with ciprofloxacin using grafted concrete demolition wastes by ATPES as reactive material: batch and modeling study," *Egyptian Journal of Chemistry*, vol. 65, no. 10, pp. 585–596, 2022, https://doi.org/10.21608/ejchem.2022.115123.5222

[54] A. F. Ali and Z. T. Abd Ali, "Interaction of aqueous Cu2+ ions with granules of crushed concrete," *Iraqi Journal of Chemical and Petroleum Engineering*, vol. 20, no. 1, pp. 31–38, 2019, https://doi.org/10.31699/IJCPE.2019.1.5

[55] A. Q. Saeed, H. M. Khudhair, A. S. H. Alhamdani, S. L. Abbas, and M. J. Abdulhasan, "Using Iron/Nickel Coated Sand Nanocomposites Prepared by Eucalyptus Leaf Extract for Copper Removal from Aqueous Solutions," *Ecological Engineering & Environmental Technology*, vol. 25, no. 7, pp. 219–224, Jul. 2024, https://doi.org/10.12912/27197050/188192

[56] M. N. Ezzat and Z. T. A. Ali, "Green approach for fabrication of graphene from polyethylene terephthalate (PET) bottle waste as reactive material for dyes removal from aqueous solution: Batch and continuous study," *Sustainable Materials and Technologies*, vol. 32, p. e00404, Jul. 2022, https://doi.org/10.1016/j.susmat.2022.e00404

[57] T. H. Mhawesh and Z. T. Abd Ali, "Reuse of brick waste as a cheap-sorbent for the removal of nickel ions from aqueous solutions," *Iraqi Journal of Chemical and Petroleum Engineering*, vol. 21, no. 2, pp. 15–23, 2020, https://doi.org/10.31699/IJCPE.2020.2.3

[58] A. M. Naji and Z. T. Abd Ali, "Evaluation of modified bentonite using chemical and physical methods for removal of amoxicillin from aqueous solutions: batch and continuous study," *Desalination and Water Treatment*, vol. 294, pp. 185–201, 2023, https://doi.org/10.5004/dwt.2023.29564

[59] Z. T. Abd Ali, H. M. Flayeh, and M. A. Ibrahim, "Numerical modeling of performance of olive seeds as permeable reactive barrier for containment of copper from contaminated groundwater," *Desalination and Water Treatment*, vol. 139, pp. 268–276, 2019, https://doi.org/10.5004/dwt.2019.23305

[60] S. D. Salman and I. M. Rashid, "Production and characterization of composite activated carbon from potato peel waste for cyanide removal from aqueous solution," *Environmental Progress & Sustainable Energy*, vol. 43, no. 1, p. e14260, Jan. 2024, https://doi.org/10.1002/ep.14260

[61] T. S. Hussein and A. A. H. Faisal, "Nanoparticles of (calcium/aluminum/CTAB) layered double hydroxide immobilization onto iron slag for removing of cadmium ions from aqueous environment," *Arabian Journal of Chemistry*, vol. 16, no. 9, p. 105031, Sep. 2023, https://doi.org/10.1016/j.arabjc.2023.105031

[62] N. F. El-Harby, S. M. A. Ibrahim, and N. A. Mohamed, "Adsorption of Congo red dye onto antimicrobial terephthaloyl thiourea cross-linked chitosan hydrogels," *Water Science & Technology*, vol. 76, no. 10, pp. 2719–2732, Nov. 2017, https://doi.org/10.2166/wst.2017.442

[63] I. W. Almanassra, V. Kochkodan, G. Ponnusamy, G. Mckay, M. Ali Atieh, and T. Al-Ansari, "Carbide Derived Carbon (CDC) as novel adsorbent for ibuprofen removal from synthetic water and treated sewage effluent," *Journal of Environmental Health Science and Engineering*, vol. 18, no. 2, pp. 1375–1390, Dec. 2020, https://doi.org/10.1007/s40201-020-00554-0

[64] K. Ebisike, A. Elvis Okoronkwo, K. Kanayo Alaneme, and O. Jeremiah Akinribide, "Thermodynamic study of the adsorption of Cd2+ and Ni2+ onto chitosan – Silica hybrid aerogel from aqueous solution," *Results in Chemistry*, vol. 5, p. 100730, Jan. 2023, https://doi.org/10.1016/j.rechem.2022.100730

[65] Q. Huang *et al.*, "Equilibrium, kinetic and thermodynamic studies of acid soluble lignin adsorption from rice straw hydrolysate by a self-synthesized macro/mesoporous resin," *RSC Advances,* vol. 7, no. 39, pp. 23896–23906, 2017, https://doi.org/10.1039/C7RA01058C

جسيمات نانوية من النحاس والزنك (nZVI-Cu) مدعمة برمل السيليكا، مُصنّعة بطريقة صديقة للبيئة لإزالة المضادات الحيوية من المحاليل المائية

فرح سمير محمد [١،*]، علاء كريم محمد [١]، زياد طارق عبد علي [٢]

١ قسم هندسة الكيمياء الحيوية، كلية هندسة الخوارزمي، جامعة بغداد، بغداد، ٤٧٠٢٤، العراق
٢ قسم هندسة البيئة، كلية الهندسة، جامعة بغداد، بغداد، ٤٧٠٢٤، العراق

الخلاصة

إزالة المضادات الحيوية من المسطحات المائية تُعد من التحديات الكبيرة، كونها من أكثر الملوثات البيئية انتشارًا، ولا سيما عند استخدام طرق المعالجة التقليدية لمياه الصرف الصحي، وذلك بسبب ثباتها العالي وانخفاض قابليتها للتحلل الحيوي. في هذه الدراسة، تم فحص استخدام الحديد الصفري النانوي (nZVI) لإزالة المضادات الحيوية من المياه.استُخدم مستخلص أوراق الكونكاربس، الغني بشكل أساسي بالمركبات الفينولية مثل الفلافونويدات والتانينات، كمصدر أخضر لتحضير جسيمات Fe/Cu النانوية، حيث يعمل كعامل اختزال صديق للبيئة. تم تثبيت الجسيمات النانوية على رمل السيليكا لتكوين متراكب نانوي من نوع SS–Fe/Cu، استُخدم لإزالة التتراسايكلين والسيبروفلوكساسين من المحاليل المائية. تمت دراسة الخصائص التركيبية للمتراكب النانوي المحضَّر باستخدام مجموعة من التقنيات التحليلية، شملت (XRD, FTIR, FE–SEM, EDS, TEM, BET, TGA, DSC). وأكدت التحاليل التركيبية والمورفولوجية نجاح تحضير متراكب SS–Fe/Cu النانوي، مع توزع جيد للجسيمات النانوية (FE–SEM/TEM)، ووجود المجاميع الوظيفية المميزة (FTIR)، والبنية البلورية (XRD)، وزيادة المساحة السطحية (BET)، والتركيب العنصري (EDS)، إضافةً إلى الاستقرار الحراري الجيد (TGA/DSC). أُجريت التجارب بطريقة الدُفعات، وتمت دراسة تأثير عدد من العوامل، مثل زمن التلامس، وقيمة الأس الهيدروجيني، وسرعة التحريك، وجرعة المتراكب النانوي، والتركيز الابتدائي للملوث .وبلغت أعلى كفاءات إزالة ٩٣٪ للتتراسايكلين و٨٥٪ للسيبروفلوكساسين تحت الظروف المثلى، وهي: زمن تلامس ٩٠ دقيقة، pH يساوي ١١ للتتراسايكلين و٧ للسيبروفلوكساسين، سرعة تحريك ٢٠٠ دورة/دقيقة، تركيز ابتدائي ١٠ ملغم/لتر، وجرعة متراكب مقدارها ١ غ/٥٠ مل. أظهرت دراسات الإيزوثيرم والحركية والثرموديناميك أن امتزاز كلٍ من التتراسايكلين والسيبروفلوكساسين يتبع نموذج فريندلخ وحركية pseudo–second، مما يدل على أن الامتزاز الكيميائي هو الآلية المسيطرة. كما بينت النتائج الثرموديناميكية أن امتزاز التتراسايكلين كان ماصًا للحرارة وغير تلقائي (ΔS° موجبة)، في حين كان امتزاز السيبروفلوكساسين طاردًا للحرارة وتلقائياً (ΔS° سالبة)، مما يؤكد كفاءة متراكب SS–Fe/Cu النانوي. تشير النتائج إلى أن متراكب SS–Fe/Cu النانوي المُحضَّر بطريقة خضراء يمكن استخدامه كعامل فعّال لإزالة التتراسايكلين والسيبروفلوكساسين من المحاليل المائية.

الكلمات الدالة: مستخلص أوراق الكونوكاربس، nZVI، مركب نانوي منSS–Fe/Cu، التتراسيكلين، السيبروفلوكساسين، الامتزاز .